Asociación Argentina
de Mecánica Computacional

Mecánica Computacional Vol XXIX, págs. 8687-8697 (artículo completo)
Eduardo Dvorkin, Marcela Goldschmit, Mario Storti (Eds.)
Buenos Aires, Argentina, 15-18 Noviembre 2010

# INVESTIGATION OF GEOLOGICAL FAULT REACTIVATION AND OPENING

**Pedro K. Nacht**[a], **Maria F. F. de Oliveira**[a], **Deane M. Roehl**[a] **and Alvaro M. Costa**[b]

[a]*Department of Civil Engineering, Computer Graphics Technology Group (Tecgraf), Pontifical Catholic University of Rio de Janeiro (PUC-Rio), Rio de Janeiro, 22453-900, Brazil, pnacht@tecgraf.puc-rio.br, mariafer@tecgraf.puc-rio.br, droehl@civ.puc-rio.br,*

[b]*Exploration and Production Business Area, Petrobras, Rio de Janeiro, Brazil. amcta@petrobras.com.br*

**Keywords:** Fault reactivation, finite element method, interface elements.

**Abstract**. The reactivation and opening of geological faults during reservoir injection is a relevant aspect in the design of injection pressures for hydrocarbon fields. As the pore pressure increases in the reservoir, the effective normal stresses on the fault's plane decrease, and as a consequence, the fault slips and reactivates. Eventually, due to increasing pore pressures, the effective normal stresses decrease to zero and the fault opens. Both phenomena are undesirable since the hydrocarbon fluid can thus migrate from the reservoir to other porous layers and/or cause surface leakage. This paper investigates a simplified analytical approach for the two-dimensional analysis of fault reactivation during reservoir injection. The pore pressure increment that causes the fault to reactivate is analytically estimated for a given reservoir thickness and depth according to the Mohr-Coulomb criterion. A parametric analysis is performed and indicates the influence of geometric parameters such as the fault's dip angle and and the reservoir's height and depth. Finally, this simplified technique is applied to a synthetic case and final results are confronted to two-dimensional finite element simulations.

## 1 INTRODUCTION

Faults are natural geological discontinuities in the upper crust. Natural resource extractions such as mining and fluid withdrawal can change the stress state near geological faults, causing them to slip and reactivate. In such cases, phenomena such as induced seismicity (Alberti, 2010), severe ground subsidence (Chan and Zoback, 2007), and fluid leakage may occur (Wiprut and Zoback, 2000), among others (Donnelly, 2009).

In the oil and gas industry, hydrocarbon recovery induces changes in the reservoir pressure during depletion and injection periods, modifying the stress state of the whole formation including nearby faults. If the stress state of a fault plane is sufficiently disturbed, the fault may slip and reactivate. In this situation, the fault's permeability is increased and its vertical seal is breached even if the fault was originally sealed by lateral juxtaposition or deformation processes.

One could cite as possible damages caused by fault reactivation: instability of wellbores, sheared-collapsed casings, fluid leakage to the surface, fluid escape to shallower porous layers, and aggravated ground subsidence. These problems can be mitigated by taking into account the reactivation tendency of mapped faults during the planning phase to better locate wells and other infra-structure. During the production and recovery phase, the maximum sustainable injection pressure should be estimated to prevent fault reactivation and preserve hydrocarbon trap integrity. Recently, special attention has been given to fault reactivation in projects for $CO_2$ sequestration in depleted reservoirs (Hawkes et al., 2005, Rutqvist et al., 2007), where the minimum horizontal stress is reduced and faults may become more prone to slip.

Fault slippage and reactivation was first recognized as a possible cause of fluid flow in faulted areas by Sibson (1990) and is fundamentally ruled by the Mohr-Coulomb criterion. This phenomenon has been extensively investigated and a detailed review is provided by Zoback (2007). Three different approaches can be found in literature: analytical, semi-analytical, and numerical.

Analytical approaches usually simplify the problem to homogeneous and regular shaped reservoirs submitted to constant pore pressure and make use of closed-form solutions that range from simple Mohr-Coulomb failure relations to fundamental solutions of elastic inclusions embedded in a halfspace (Geertsma, 1966, 1973; Segall, 1989, 1992; Zoback, 2007; Soltanzadeh and Hawkes, 2009). Despite simplifying the pore pressure-stress coupling to some degree in the reservoir and/or in the fault (Hillis, 2001), the simplest analytical procedures seems to be the most popular choices for a first analysis. Some applications can be found in Moeck et al. (2009) and Neves et al. (2009).

Semi-analytical approaches employ the aforementioned fundamental solutions to estimate reactivation of faults crossing reservoirs with irregular shapes and spatially variable pore pressures (Chanpura and Germanovich, 2001; Zoback, 2007; Soltanzadeh and Hawkes, 2008). At the cost of manipulating more complex expressions, the pore pressure-stress coupling is better accounted for. A common practice is to obtain the pore pressure distribution and the stress evolution from flux and stress analyses, either coupled or uncoupled, to use as an input to analytical and semi-analytical relations.

Numerical approaches can better approximate the geometry and the property heterogeneity of the field. The fault is represented in the discrete models as either a discontinuous surface with relative displacements or a continuous band with weakened properties. Applications employ a variety of numerical techniques such as the finite element method (FEM) (Vidal-Gilbert, 2009; Zhang et al., 2009), the finite difference method (FDM) (Rutqvist et al., 2007;

Zhang et al., 2009; Fouladvand et al., 2009) and the discrete element method (DEM) (Zhang and Sanderson, 1996; Langhi et al., 2009).

This work investigates a simplified analytical approach for two-dimensional analysis of fault reactivation under normal stress regime according to the Mohr-Coulomb criterion, based on the fault's orientation and the field's initial stress state. The pore pressure increment that causes a given fault to reactivate during injection is estimated by the simplified analytical approach for a variety of reservoir thicknesses and depths and is confronted with FEM results for a synthetic model. The comparison shows how effectively the simplified analytical approach estimates fault reactivation.

## 2 FAULT REACTIVATION AND OPENING

Faults can be classified according to Anderson's scheme (Zoback, 2007) as normal (or extensional), strike-slip and reverse (or thrust) as a function of the vertical stress ($\sigma_v$) and the minimum and maximum horizontal stresses ($\sigma_h$ and $\sigma_H$), as depicted in Figure 1.

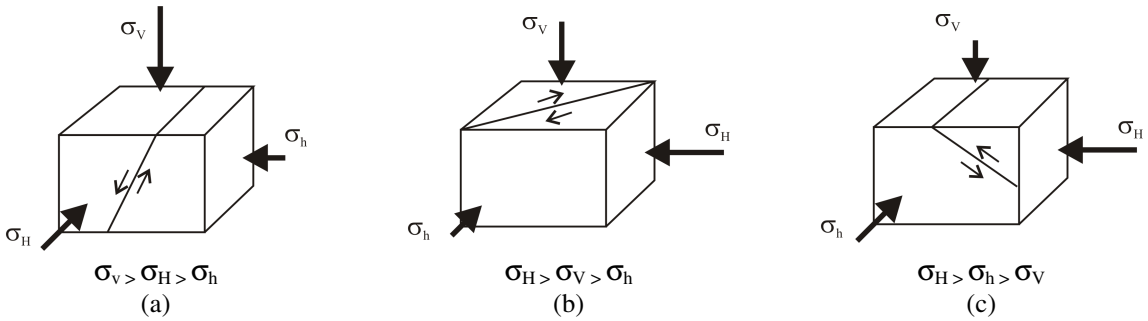


Figure 1: Anderson's classification: a) normal fault; b) strike-slip fault; c) reverse fault.

Fault reactivation is controlled by the shear and normal stress components on the fault plane, which can be expressed for a normal faulting regime in the two-dimensional case as

$$\tau = \frac{1}{2}(\sigma_V - \sigma_h)\sin(2\theta) \tag{1}$$

$$\sigma_n = \frac{1}{2}(\sigma_V + \sigma_h) + \frac{1}{2}(\sigma_V - \sigma_h)\cos(2\theta) \tag{2}$$

where $\theta$ is the fault's dip angle. It is assumed that the fault's strength behaves according to the Mohr-Coulomb criterion

$$\tau_{slip} = c + \mu(\sigma_n - \alpha p) \tag{3}$$

where $p$ is the pore pressure, $\alpha$ is Biot's coefficient, $c$ is the fault's cohesion and $\mu = \tan\phi$ is the fault's friction coefficient for a given fault's friction angle $\phi$. In the above expression $\sigma_n - \alpha p = \sigma'_n$ is the effective normal stress on the fault plane. The likelihood of reactivation for a given fault can be measured by the modified slip tendency parameter

$$ST = \frac{\tau}{\tau_{slip}} \tag{4}$$

ranging within $0 \le ST \le 1$. The higher the slip tendency parameter is, the more susceptible to

reactivation the fault becomes.

Field observations suggest that faults become hydraulically conductive when the shear stress $\tau$ violates the Mohr-Coulomb envelop. Byerlee (1978) found that hydraulically active faults have friction coefficients within $0.6 \leq \mu \leq 1.0$ ($31^\circ \leq \phi \leq 45^\circ$), although faults containing clay minerals may have lower values. The fault's cohesion is usually lower than 1 MPa and commonly taken as null. Applying Eq. (4) for cohesionless faults with friction coefficient $\mu \sim 0.6$, one obtains that normal faults with dip angle $\theta \sim 60^\circ$ are more prone to reactivate.

Besides the knowledge of the fault's properties, a proper estimation of the sustainable pore pressure to prevent fault reactivation depends on the stress and fluid paths of the reservoir (Hillis, 2001; Streit, 2002). Since the vertical stress $\sigma_V$ is strongly related to the weight of the overburden and the crust is not vertically restrained, this stress component is little affected by the pore pressure changes in the reservoir. On the other hand, the reservoir is constrained in the horizontal direction and the horizontal stress $\sigma_h$ can be largely affected by pore pressure changes. According to Hillis (2001), the change in the horizontal stress $\sigma_h$ can be inferred from production data or estimated from analytical expressions from idealized elastic reservoirs.

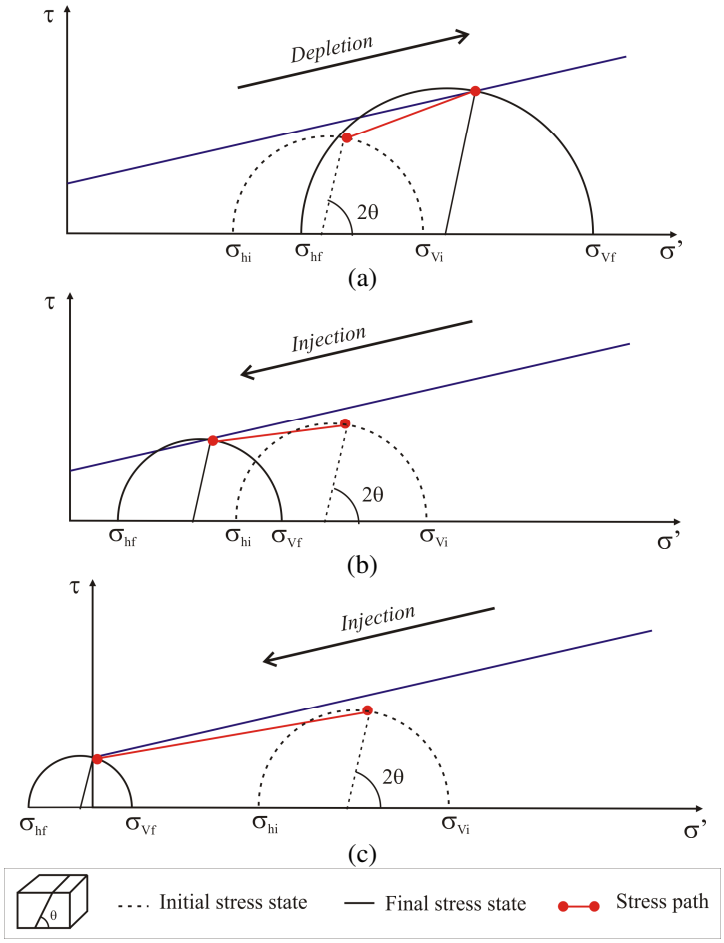


Figure 2: Mohr-Coulomb diagram for: a) a reactivated fault during depletion; b) a reactivated fault during injection; c) an open fault during injection.

During depletion, the horizontal stress $\sigma_h$ decreases and thus increases the difference $\sigma_V - \sigma_h$. As a consequence, the fault can reactivate despite the increase in the effective stresses, as

shown in Figure 2(a). On the other hand, during injection, the horizontal stress $\sigma_h$ increases and thus reduces the difference $\sigma_V - \sigma_h$, as depicted in Figure 2(b)–(c). In this case, the fault can reactivate if the shear stress reaches the failure envelope and/or open if the effective normal stress is reduced to zero, as shown in Figures 2(b) and 2(c), respectively. Note that, depending on the fault's properties and orientation, it is possible for a fault to open before reactivating and thus admit fluid flow.

## 3 MAXIMUM SUSTAINABLE INJECTION PRESSURE TO PREVENT FAULT REACTIVATION

### 3.1 Simplified analytical approach

During injection, a simplified estimative of the required pore pressure to induce fault reactivation can be obtained by disregarding changes in the vertical and horizontal stresses. Then, an explicit expression for pore pressure can be found by solving Eq. (4) for $p$ when $ST = 1$. In this case, the Mohr's circle moves towards the origin without changes in size, as shown in Figure 3.

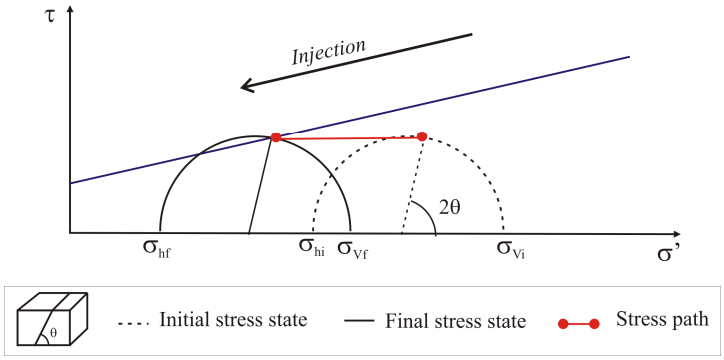


Figure 3: Mohr-Coulomb diagram for a reactivated fault during injection considering the simplified analytical approach.

### 3.2 Finite element modeling approach

A two-dimensional discrete FE model comprised by the stratigraphic horizons and the geological faults can simulate the changes in the stress state during injection more precisely, in particular in the horizontal stresses. In this work, the finite element simulations were carried out by using the program AEEPECD® (Costa, 1984), developed in Petrobras for two-dimensional analyses in terms of effective stresses under drained conditions.

Rocks were modeled by quadratic quadrilateral 8-node serendipity finite elements. Non-reservoir and reservoir rocks were assumed to behave according to the elastoplastic and poro-elastoplastic Mohr-Coulomb constitutive model, respectively, with associated flow rule and zero tensile cut-off.

Faults were modeled by quadratic interface (or joint) 8-node elements (Goodman, 1968). The shear and normal stresses are related to their corresponding relative displacements by the tangential and normal stiffness of the fault's core, which are taken as

$$K_n = \frac{E}{t} \quad \text{and} \quad K_t = \frac{E}{2(1-\nu)\,t} \tag{5}$$

where $E$ and $\nu$ are the Young's elasticity modulus and the Poison's ratio of the adjacent geological layer, respectively, and $t$ is the thickness of the fault core. A poro-elastoplastic Mohr-Coulomb constitutive model, with associated flow rule and zero tensile cut-off, simulated the behavior of the effective normal and shear stresses ($\sigma'_n$ and $\tau$) along the fault.

Fault extensions intersecting the reservoir are considered initially non-sealed and the extensions outside the reservoir are considered horizontally sealed during the whole analysis. Pore pressure simulates the effect of internal fluid pressure acting on the fault extensions that are hydraulically connected to the pressurized reservoir, i.e., the fault extensions that either are initially non-sealed or have already been reactivated. Only the effective normal stress components are directly affected by the pore pressure increments.

In-situ vertical and horizontal stresses were modeled as initial geostatic stresses varying with depth.

## 4 RESULTS AND DISCUSSION

The two-dimensional case of a normal fault was investigated, as depicted in Figure 4. For convenience, a reference model is defined, with dip angle $\theta = 45°$ intersecting a reservoir with thickness of $t_r$ = 100 m at the depth $H$ = 1200 m. Rock properties are provided in Table 1, in which $E$ is the Young's elasticity modulus, $\nu$ is the Poisson's ratio, $c$ is the cohesion, $\phi$ is the friction angle and $\alpha$ is Biot's coefficient. Values of cohesion $c$ = 0.5 MPa and friction angle $\phi = 20°$ are adopted for the fault, whose normal and tangential stiffness are obtained by applying Eq. (5) for a thickness of 0.5 m.

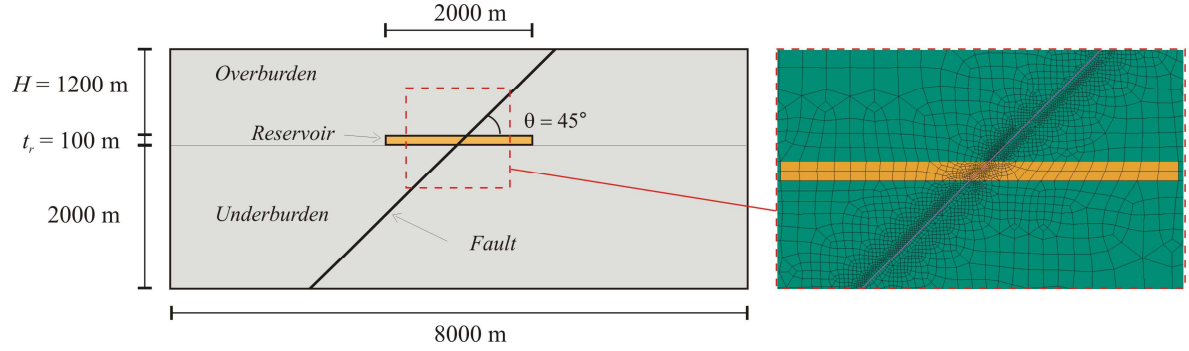


Figure 4: Two-dimensional case of a normal fault investigated by the simplified analytical approach and the FE modeling approach: (a) geometrical model; b) detail of the FE mesh.

| *Layer* | *E* (GPa) | ν | *c* (MPa) |
|---|---|---|---|
| Overburden | 17.0 | 0.30 | 1.5 |
| Reservoir | 15.0 | 0.25 | 2.0 |
| Underburden | 17.0 | 0.30 | 1.5 |

Table 1: Rock property values for the two-dimensional reference model of a normal fault.

The initial stress state can be obtained as

$$\sigma_V = \gamma H \quad \text{and} \quad \sigma_h = K_0 \, \sigma'_V \tag{6}$$

where $\gamma$ is the unit weight and $K_0$ is the lateral earth pressure coefficient, which assume the values 22.5 kN/m$^2$ and 0.5, respectively, for the reference model. The initial pressure

distribution in the reservoir is considered constant and hydrostatic; pore pressure was incremented in steps of 100 kPa.

The fault reactivation was analyzed for the reference model by applying the simplified analytical approach and the FE modeling approach, briefly described in the previous section. According to the analytical approach, a pore pressure increment of 2.32 MPa induces fault reactivation, opposed to an increment of 2.60 MPa obtained from the numerical simulation. The discrepancy of about 12% can be visualized in the Mohr's diagram, shown in Figure 5. It becomes evident how disregarding the changes in the minimum horizontal stress due to deformation affects the results.

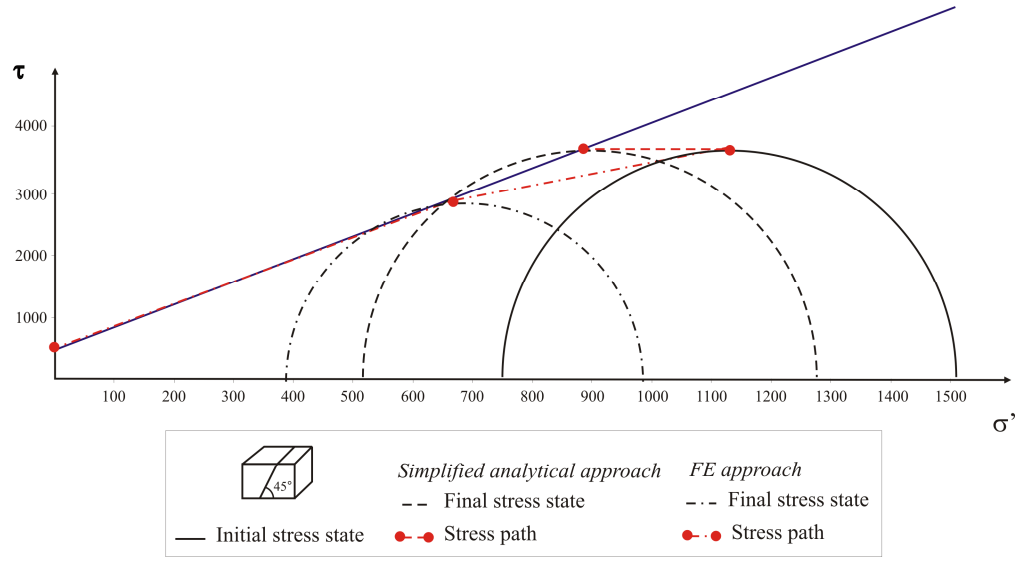


Figure 5: Mohr's diagram during injection for the reference model of a normal fault with dip angle $\theta = 45°$.

## 4.1 Parametric analysis

A parametric analysis was carried out on the geometry configuration of the reference model. The reservoir's depth and thickness as well as the fault's dip angle were varied according to Table 2, leading to a total of 27 analyses.

| $\theta$ (°) | $H$ (m) | $h_r$ (m) |
|---|---|---|
| 30 | 400 | 20 |
| 45 | 1200 | 100 |
| 60 | 2000 | 180 |

Table 2: Values of the fault's dip angle and the reservoir's depth and thickness varied in the parametric analyses.

The FE incremental analyses were carried out until the fault opened ($\sigma'_n=0$) and results are presented in Table 4. Fault reactivation occurred before opening in all of the cases. It was found that, in the cases where similar pore pressure values for reactivating and opening the fault were obtained, only short lengths of the fault had experienced reactivation by the time opening took place, as shown in Figure 6(a) for case 1. Conversely, when this difference was pronounced, long lengths of the fault had been reactivated by the time the fault opened, as shown in Figure 6(b) for case 22. Ultimately, the whole length of the fault reactivated without opening in situations such as cases 18, 26 and 27.

| *Case* | $\theta$ (°) | *Parameters* | | $\Delta p$ (kPa) | |
|---|---|---|---|---|---|
| | | *H* (m) | *hr* (m) | *Reactivation* | *Opening* |
| 1 | 30 | 400 | 20 | 2400 | 2400 |
| 2 | | | 100 | 2400 | 2400 |
| 3 | | | 180 | 2300 | 2400 |
| 4 | | 1200 | 20 | 5100 | 7000 |
| 5 | | | 100 | 5000 | 7100 |
| 6 | | | 180 | 4800 | 6900 |
| 7 | | 2000 | 20 | 7600 | 11700 |
| 8 | | | 100 | 7400 | 11400 |
| 9 | | | 180 | 7200 | 10900 |
| 10 | 45 | 400 | 20 | 1900 | 2300 |
| 11 | | | 100 | 1800 | 2300 |
| 12 | | | 180 | 1700 | 2200 |
| 13 | | 1200 | 20 | 2600 | 6100 |
| 14 | | | 100 | 2600 | 5600 |
| 15 | | | 180 | 2500 | 5800 |
| 16 | | 2000 | 20 | 3300 | 9200 |
| 17 | | | 100 | 3200 | 9200 |
| 18 | | | 180 | 3100 | - |
| 19 | 60 | 400 | 20 | 1800 | 2100 |
| 20 | | | 100 | 1700 | 2100 |
| 21 | | | 180 | 1600 | 2000 |
| 22 | | 1200 | 20 | 2100 | 6000 |
| 23 | | | 100 | 2200 | 5100 |
| 24 | | | 180 | 2100 | 5100 |
| 25 | | 2000 | 20 | 2400 | 7600 |
| 26 | | | 100 | 2500 | - |
| 27 | | | 180 | 2400 | - |

Table 4: Pore pressure increment that reactivates and opens the fault obtained from the FEM analyses

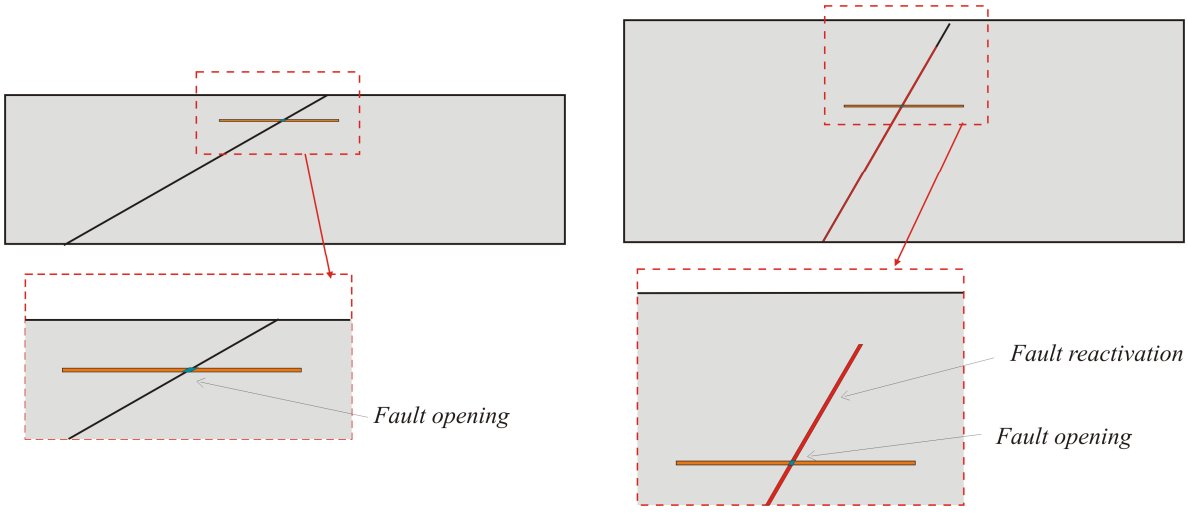


(a) Case 1 (b) Case 22

Figure 6: Fault reactivation by the time the opening occurs (reactivation in red, opening in blue): a) case 1; b) case 22.

Figures 7 and 8 show the pore pressures that reactivate the fault for variations of the fault's dip angle and the reservoir's depth, respectively. Note the small influence of the reservoir's thickness in comparison to other parameters.

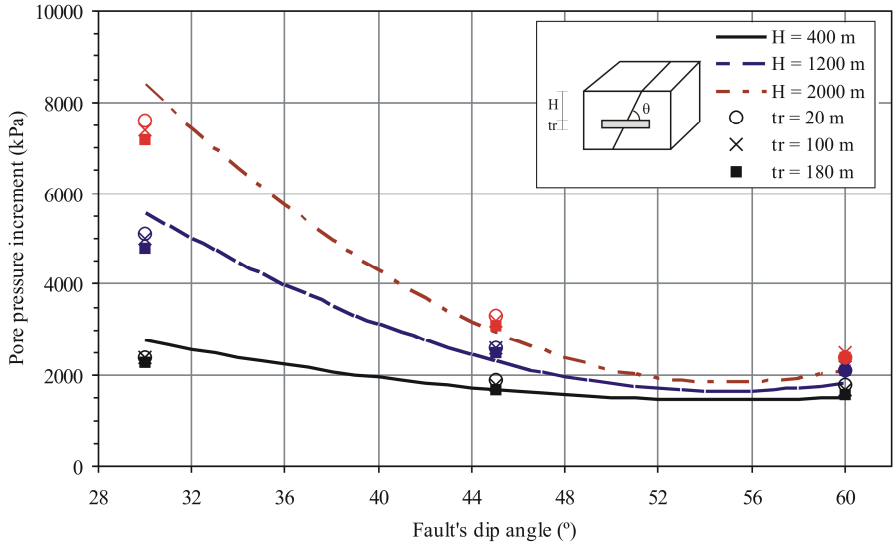


Figure 7: Pore pressure increment that reactivates the fault of the reference model for different values of dip angle.

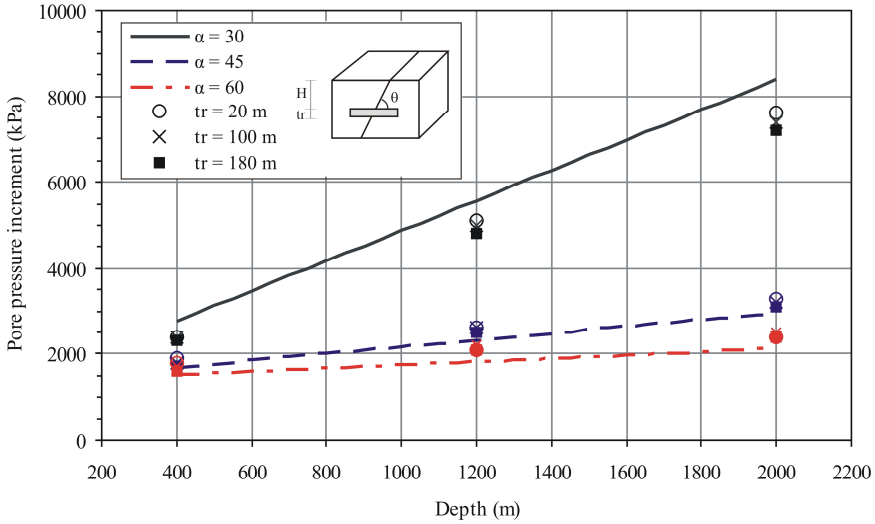


Figure 8: Pore pressure increment that reactivates the fault of the reference model for different values of depth.

## 5 CONCLUDING REMARKS

This work investigated reactivation and opening of faults under normal stress regime by applying a simplified analytical approach and the FE modeling approach. A parametric analysis studied the influence of the fault's dip angle and the reservoir's thickness and depth on the required pore pressure increment to induce fault reactivation.

The difference in results obtained by the analytical and the FE approach shows that deformation caused by pore pressure-stress coupling can be substantial for some situations and should not be disregarded. A better prediction could be obtained by enriching the

analytical relations with other terms that take into account the reservoir deformation.

Nevertheless, the simplified analytical approach can be a powerful tool for a first analysis and can be used together with a flux simulator to identify the most critically stressed faults in a field. The results can assist the selection of areas for which a more detailed and time-consuming numerical analysis should be carried out.

## ACKNOWLEDGEMENTS

This work was supported by Petrobras S.A and National Council for Scientific and Technological Development (CNPq/PIBIC), Brazil.

## REFERENCES

Addis, M. A. et al., The influence of the reservoir stress-depletion response of the lifetime considerations of well completion design.

Alberti, M., Analysis of kinematic correlations in faults and focal mechanisms with GIS and Fortran programs. *Computers & Geosciences*, 36–186:194, 2010.

Byerlee, J., Friction of rocks. *Pure Applied Geophysics*, 116:615–626, 1978.

Chan, A.W. and Zoback, M.D., The role of hydrocarbon production of land subsidence and fault reactivation in the Lousiana coastal zone. *Journal of Coastal Research*, 23:771-786, 2007.

Chanpura, R.A. and Germanovich, L.N., Faulting and seismicity associated with fluid extraction. In: *Rock Mechanics in the National Interest* (Eds. Tinucci and Heasley), Swets & Zeitlinger Lisse, 2001.

Costa, A.M., An application of computational methods and principles of rock mechanics in the design and analysis of underground excavations for the underground mining. *PhD Thesis*, Graduate School of Engineering (COPPE), Federal University of Rio de Janeiro (UFRJ), 1984.

Donnelly, L.J., A review of international cases of fault reactivation during mining, subsidence and fluid abstraction. *Quarterly Journal of Engineering Geology and Hydrogeology*, 42:73–94, 2009.

Fouladvand, A. et. al., Geomechanical modeling integrating subseismic faults. In: *SPE Asia Pacific Oil and Gas conference and Exhibition*, Society of Petroleum Engineering, 2009.

Geerstsma, J., Land subsidence above compacting oil and gas reservoirs. *Journal of Petroleum Technology*, 25:734–744, 1973.

Geertsma, J., Problems of rock mechanics in petroleum production engineering. In: *First Congress of the International Society of Rock Mechanics*, 585–594, 1966.

Goodeman, R.E. et al., A model for the mechanics of jointed rocks. *ASCE Journal of Soil Mechanics Found. Div.*, 94:637–659, 1968.

Guimarães, L.J.N. et al., Influence of mechanical constitutive model on the coupled hydro-geomechanical analysis of fault reactivation. In: *SPE Reservoir Simulation Symposium*, Society of Petroleum Engineering, 2009.

Hawked, C.D. et al., Geomechanical factors affecting geological storage of $CO_2$ in depleted ir and gas reservoirs. *Journal of Canadian Petroleum Technology*, 44:52–61, 2005.

Hillis, R. R., Coupled changes in pore pressure and stress in oil fields and sedimentary basins. *Petroleum Geoscience*, 7:419–425, 2001.

Hunt, S.P. et al., A new geomechanical tool for the evaluation of hydrocarbon trap integrity. In: *41st U.S. Symposium on Rock Mechanics*, American Rock Mechanics Association (ARMA), 2005.

Langhi, L. et al., Evaluating hydrocarbon trap integrity during fault reactivation using geomechanical three-dimensional modeling: An example from the Timor Sea, Australia. *AAPG Bulletin*, 94:567–591, 2009.

Moeck, I. et al., Slip tendency analysis, fault reactivation potential and induced seismicity in a deep geothermal reservoir. *Journal of Structural Geology*, 31:1174–1182, 2009.

Neves, M.C. et al., Software for slip-tendency analysis in 3D: A plug-in for Coulomb. *Computers & Geosciences*, 35:2345–2352, 2009.

Rutqvist, J. et al., Estimating maximum sustainable injection pressure during geological sequestration of $CO_2$ using coupled fluid flow and geomechanical fault-slip analysis. *Energy Conversion and Management*, 48:1798–1807, 2007.

Segall, P., Earthquakes triggered by fluid extraction. *Geology*, 17:942–946, 1989.

Segall, P., Induced stresses due to fluid extraction from axisymmetric reservoirs. *Pure Applied Geophysics,* 139:535–560, 1992.

Sibson, R.H., Faulting and fluid flow. In: *Short Course on Fluids in Tectonically Active Regions of the Continental Crust,* (Ed. Nerbitt, B.E.), 18:93–132, Mineralogical Association of Canada Handbook, 1990.

Soltanzadeh, H. and Hawkes, C.D., Assessing fault reactivation tendency within and surrounding porous reservoirs during fluid production or injection. *International Journal of Rock Mechanics & Mining Sciences*, 46:1–7, 2009.

Soltanzadeh, H. and Hawkes, C.D., Semi-analytical models for stress change and fault reactivation induced by reservoir production and injection. *Journal of Petroleum Science and Engineering*, 60:71–85, 2008.

Streit, J.E. and Hillis, R.R., Estimating fluid pressures that can induce reservoir failure during hydrocarbon depletion. In: *SPE/ISRM Rock Mechanics Conference*, Society of Petroleum Engineers, 2002.

Vidal-Gilbert, S. et al., 3D geomechanical modeling for $CO_2$ geologic storage in the Dogger carbonates of the Paris Basin. *International Journal of Greenhouse Gas Control*, 3:288–299, 2009.

Wiprut, D. and Zoback, M.D., Fault reactivation and fluid flow along a previously dormant normal fault in the northern North Sea. *Geology*, 28:595–598, 2000.

Zhang, X. and Sanderson, D.J., Numerical modeling of the effects of fault slip on fluid flow around extensional faults. *Journal of Structural Geology*, 18:109–119, 1996.

Zhang, Y. et. al., Numerical modeling of strain localization and fluid flow during extensional fault reactivation: Implications for hydrocarbon preservation. *Journal of Structural Geology*, 31:315–327, 2009.

Zoback, M.D., *Reservoir geomechanics*, Cambridge University Press, 2007.